Theoretical study of lithium graphite. II. Spatial distribution of valence electrons

N. A. W. Holzwarth, L. A. Girifalco, and S. Rabii

Departments of Physics, Electrical Engineering and Science, Metallurgy and Materials Science, and Laboratory for Research on the Structure of Matter, University of Pennsylvania, Philadelphia, Pennsylvania 19104

(Received 8 May 1978)

Based on band-structure calculations presented in part I, the valence charge density of LiC_6 is evaluated and presented in contour diagrams and linear plots. The hybridization of the Li $2s$ states with the bands of graphite is studied and quantified in terms of the Li contact density. It is found that the Li contact density of 0.15 electrons/a.u.^{3} is mainly contributed by the bonding C π band and only 6% by the weakly antibonding Fermi-level band, as is consistent with the experimental value of the ^{7}Li Knight shift.

I. INTRODUCTION

In paper I,[1] we presented results of a detailed band-structure calculation for LiC_6. We found that the occupied bands of LiC_6 are essentially those of graphite with A-A layer stacking. The conduction bands are formed from the π bands of graphite with an excess of $\frac{1}{6}$ electron/(C atom), making LiC_6 a π-band metal. An s-like band derived from the Li $2s$ state is completely unoccupied, lying at least 1.7 eV above the Fermi level. The Li $2s$ state hybridizes to a small extent with a low-lying bonding π band of graphite; but to a negligible extent with the Fermi-level bands. To discuss these hybridization trends on a more quantitative basis and, more generally, to discuss physical properties of this π-band metal, we have evaluated the partial and total charge densities of the occupied bands of LiC_6 (excluding core-electron contributions). A knowledge of these quantities also enables us to discuss how the results of a self-consistent calculation would differ from the present results which are based on the ionic potential "$Li^+C_6^-$",[1] and enables us to make qualitative statements about cohesive properties[2] of LiC_6. Contact can be made with experimental nuclear-magnetic-resonance (NMR)[3] and phonon Raman spectra.[4]

Paper II[5] is organized as follows: In Sec. II the numerical methods used to generate the charge densities are discussed; in Sec. III the total and partial charge densities are presented in the form of contour plots. The amount of Li hybridization is quantified in terms of the Li contact density. Qualitative remarks about bonding characteristics and comparison with experiment are included. In Sec. IV, we attempt to understand the hybridization trends from energetic considerations which are then used to discuss differences between LiC_6 and other donor intercalation compounds. Section IV also includes a brief discussion of the self-consistency of the present results and general conclusions.

II. NUMERICAL METHODS

The charge densities presented in this paper are based on the band-structure calculations[1] for the potential $Li^+C_6^-$. The electronic charge density for a band α is given by

$$\rho_\alpha(\vec{r}) = 2\frac{\Omega}{(2\pi)^3}\int_{BZ} d^3k\,\Theta(E_F - E_\alpha(\vec{k})) \times |\Psi_\alpha(\vec{k},\vec{r})|^2 \ . \quad (1)$$

Here Ω denotes unit-cell volume, Θ is a step function, $E_\alpha(k)$ is the band energy derived from the solution of Eq. (4) of Paper I, and $\Psi_\alpha(\vec{k},\vec{r})$ is the corresponding wave function evaluated according to Eq. (2) of Paper I. The evaluation of the muffin-tin basis functions $\psi(\vec{k},\vec{r})$ which compose $\Psi_\alpha(\vec{k},\vec{r})$ is described in the Appendix of Paper I. For the fully occupied bands and as an approximation to the partly occupied bands, the partial charge density (1) can be written in terms of an integral over the entire Brillouin zone

$$\rho_\alpha(\vec{r}) = O_\alpha\frac{\Omega}{(2\pi)^3}\int_{BZ} d^3k\,|\Psi_\alpha(\vec{k},\vec{r})|^2 \ . \quad (2)$$

Here the occupancy O_α is 2 for the fully occupied bands and more generally,

$$O_\alpha = 2\frac{\Omega}{(2\pi)^3}\int_{BZ} d^3k\,\Theta(E_F - E_\alpha(\vec{k})) \ . \quad (3)$$

For the partially occupied bands, the values of O_α were estimated by evaluating (3) via an LCAO interpolation as discussed in Sec. V of Paper I; the resultant values are listed in Table III of Paper I. The Brillouin-zone integrals (2) were evaluated by a special-point integration procedure[6] using the single special point $\vec{k}_0 = \frac{2}{3}\vec{\Gamma M} + \frac{1}{2}\vec{\Gamma A}$. This choice of special point is such, that if the integrand is expressed in terms of a Wannier expansion,[6] all

terms corresponding to lattice translations in the first three shells, having lengths $\lesssim 10.7$ a.u., are treated exactly. The first neglected lattice translations have lengths $\gtrsim 14.0$ a.u. Unfortunately, without further work, it is not possible to estimate the error introduced by evaluating Eq. (2) by this special-point procedure, nor the error introduced by approximating the density (1) of the partially filled bands by the Brillouin-zone integral (2). However, we expect that the qualitative features of the charge density are properly determined by the present approximate treatment.

III. TOTAL AND PARTIAL VALENCE-ELECTRON CHARGE DISTRIBUTIONS

It was suggested in I,[1] on the basis of the form of the band structure, that the 25 valence electrons of LiC_6 are accommodated in bands characteristic of graphite having A-A layer stacking; nine σ bands and five π bands. The highest two π bands contain one electron and correspond to unoccupied weakly antibonding states of graphite. The remaining 12 bands are fully occupied and correspond to the occupied states of graphite. It will be seen that the forms of the total and partial valence-charge distributions are consistent with this picture.

Contour plots of total and partial valence-electron charge densities of LiC_6 were constructed in the five planes $z = 0$ (Li plane), $\frac{1}{8}c$, $\frac{1}{4}c$ (mid plane), $\frac{3}{8}c$, and $\frac{1}{2}c$ (C plane), in the sectors shown in Fig. 1. The large triangular sector illustrates the nearest in-plane Li-Li bond in the $z = 0$ plane and the two types of nearest C-C bonds in the $z = \frac{1}{2}c$ plane. The crystal structure of LiC_6 is such that the point symmetry of each Li site is D_{6h} (12-fold symmetry within a layer) and of each C site is C_{2v} (two-fold symmetry within a layer). The small triangular sector shown in Fig. 1 contains two irreducible sectors and can generate any larger sector by 60° rotations.

Contour plots of the total valence-electron charge density are shown in the large triangular sector in Fig. 2. To compare the charge density of LiC_6 with that of A-A graphite, one may be guided by such qualitative features as the trigonal symmetry of the charge density with respect to a C c axis (e.g., c axis passing through a carbon site) and the concentration of charge near the carbon layers. It is evident from Fig. 2 that the trigonal symmetry of a C c axis is essentially preserved in LiC_6 except near the Li site. The distortion of charge toward the Li site indicates the extent of Li 2s hybridization in the occupied states of LiC_6. The contour plots for the $z = \frac{1}{2}c$ (C plane) and $\frac{3}{8}c$ planes exhibit perfect trigonal symmetry with respect to a C c axis, within the

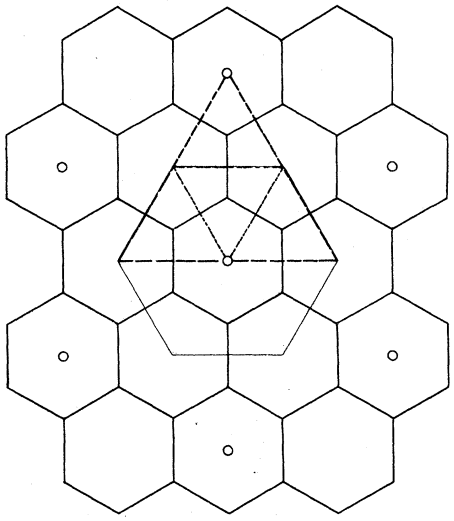

FIG. 1. c-axis projection of LiC_6 structure showing location of Li atoms (○) and C–C bonds (full lines). Contour plots for the total density (Fig. 2) is given in large triangular sector denoted by dashed lines. Contour plots of partial charge densities (Figs. 5 and 6) are given in small triangular sector denoted by dotted lines. Drawing of thee-dimensional unit cell for LiC_6 is given in Fig. 1(b) of Paper I.

accuracy of the plots. Contour plots for the $z = \frac{1}{4}c$, $\frac{1}{8}c$, and 0 planes show increasing amounts of charge attraction toward the Li site, relative to that of the $z = \frac{1}{2}c$ (C) plane. It is also evident from Fig. 2 that most of the valence electrons in LiC_6 are concentrated near the C plane, as should be expected for a graphitelike material. Since LiC_6 has 25 valence electrons per unit cell, the average valence density is 0.06 e/a.u.^{3}. With the exception of a small region near a Li site, the density throughout at least one-half of the unit cell including the volume between two midplanes enclosing a Li plane, is substantially less than the average value.

A distinctive characteristic of the valence charge distribution is its form near the Li and C sites. In Fig. 3 the charge density is plotted along the c axis starting at the Li site ($z = 0$) and extending to the C plane ($z = \frac{1}{2}c$) where it intersects the center of a C hexagon. Figure 3 shows that the density near the Li site exhibits a cusp and a minimum which is characteristic of a Li 2s orbital, the minimum occurring at a distance within 0.1 a.u. of the node of the atomic Li 2s wave function.[7] The density at the Li nucleus is found to be 0.15 e/a.u.^{3} which is the same order of magnitude of, although smaller than, the corresponding atomic value—0.21 e/a.u.^{3}.[7] Although the form of the charge density near the Li nucleus indicates the presence of Li 2s character in the occupied

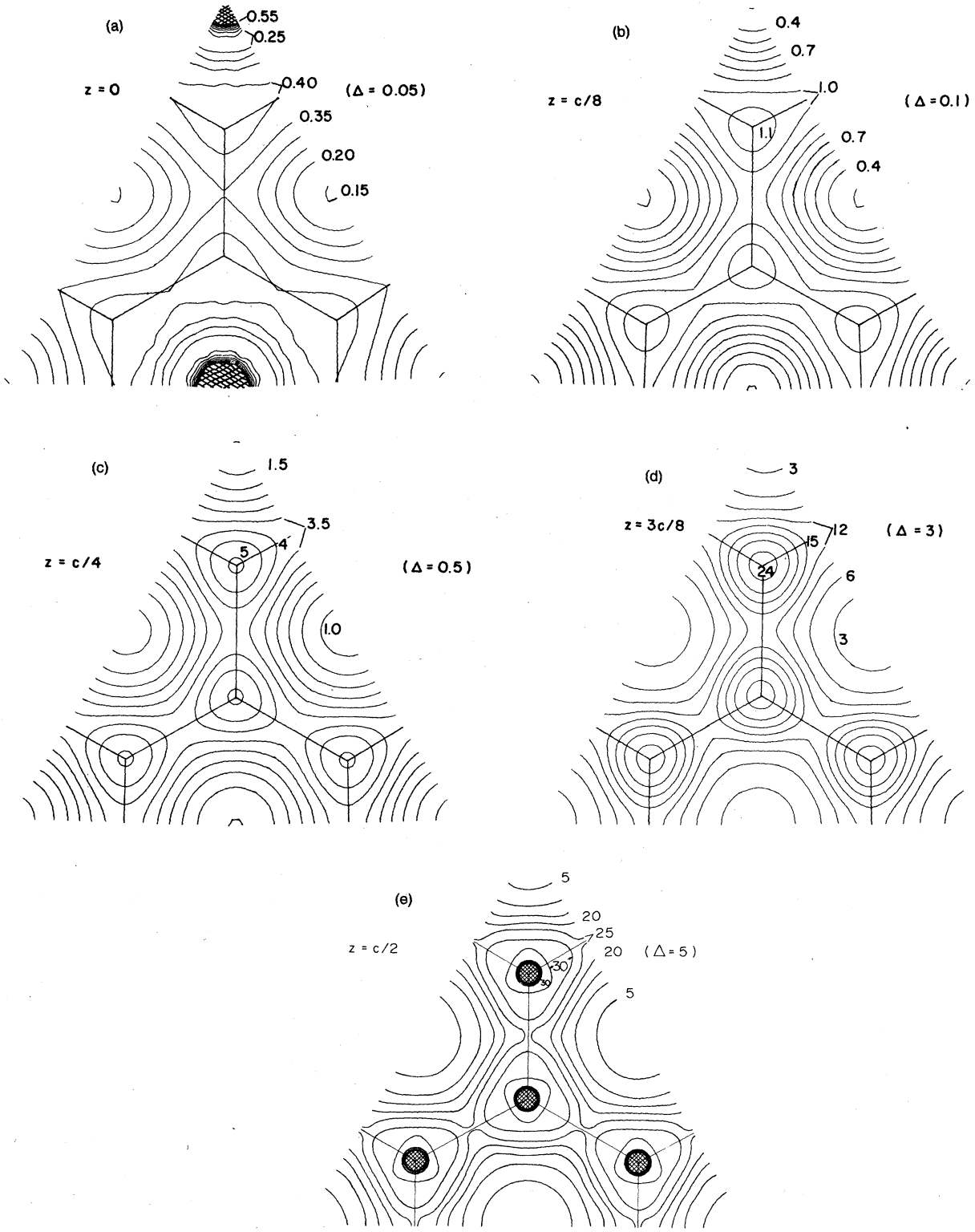

FIG. 2. Contour plots of total valence charge density in units 10^{-2} e/a.u.^{3} within large sector shown in Fig. 1 and in planes as indicated. Contours are equally spaced at intervals Δ. The plot in the C plane was generated by visual interpolation; all other plots were generated by standard computer algorithms. The crosshatched lines replace the high density of contour lines near the Li and C sites.

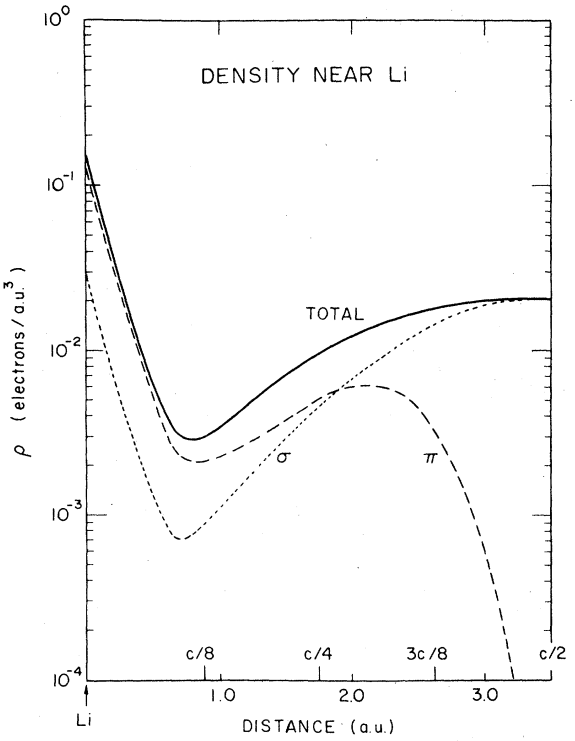

FIG. 3. Semilog plot of total valence charge density of LiC_6 along c axis starting at a Li site ($z=0$) and extending to the C plane ($z=\frac{1}{2}c$). π (dashed line) and σ (dotted line) partial densities are also indicated.

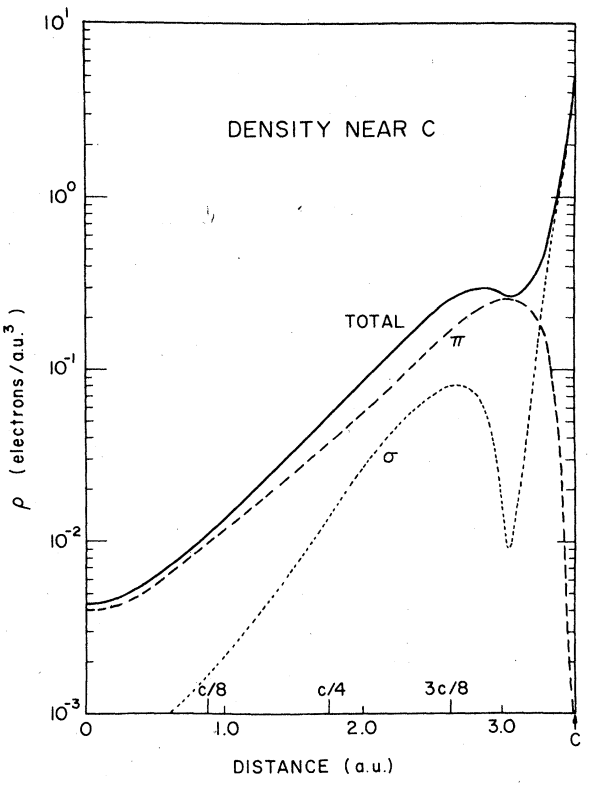

FIG. 4. Semilog plot of total valence charge density of LiC_6 (full line) along c axis starting in the Li plane ($z=0$) and extending to a C site ($z=\frac{1}{2}c$). π (dashed line) and σ (dotted line) partial densities are also indicated.

states of LiC_6, the amount of accumulated charge within 0.75 a.u. of the Li nucleus is only $\approx 10^{-2}$ e and is thus itself not effective in screening the Li^+ ion. The degree of ionization of the Li atom in LiC_6 will be discussed briefly in Sec. IV. The concentration of charge near a graphite layer is seen in more detail in Fig. 4 where the total valence charge density is plotted along the c axis starting in the Li plane ($z=0$) and extending to a C site ($z=\frac{1}{2}c$). The charge density at the C nucleus, 4.55 e/a.u.^{3}, is the same order of magnitude of, although larger than, the corresponding atomic C $2s^1$ contact density of 3.1 e/a.u.^{3} (Ref. 7). The charge density near the C site in both the C plane and parallel to the c axis exhibits a double-peaked structure characteristic of a $2sp_{xy}^2$ hybrid wave-function component.

It is instructive to consider the separate contributions from the C σ and π bands. The mixing between C σ and π bands in the occupied states of LiC_6 is very small as evidenced by the fact that the π band density in the C plane is at maximum only 10^{-3} e/a.u.^{3}. In Figs. 3 and 4 C σ- and π-band contributions to the total valence density parallel to the c axis are presented, passing through the Li and C sites, respectively. Figure 3 shows that near the Li site, the C π-band contribution to the density is at least 5 times greater than that of the C σ-band contribution. The density along the direction presented in Fig. 3 has increasing C σ-band contribution near the C plane; the C π-band contribution starting to decrease near $z=\frac{5}{16}c$. Figure 4 shows that near the C site, the charge density is dominated by the C σ-band contribution, which has the pronounced double-peaked structure characteristic of the C $2sp_{xy}^2$ hybrid wave function. The C π-band component shown in Fig. 4 has a maximum density at a distance of 0.5 a.u. from the C nucleus and dominates the total charge distribution below the C site in all planes given in Fig. 2 except the C plane. It is this relatively larger spatial extent of the C π components that favors hybridization with the Li $2s$ states over that of the C σ components. These points are illustrated further in Fig. 5 where separate contour plots of π and σ partial charge densities are given within the small triangular sector denoted in Fig. 1 in the planes $z=0$ (Li plane), $\frac{1}{8}c$, $\frac{1}{4}c$, (midplane), and $\frac{3}{8}c$. The $z=\frac{1}{2}c$ (C) plane contours are not presented in Fig.

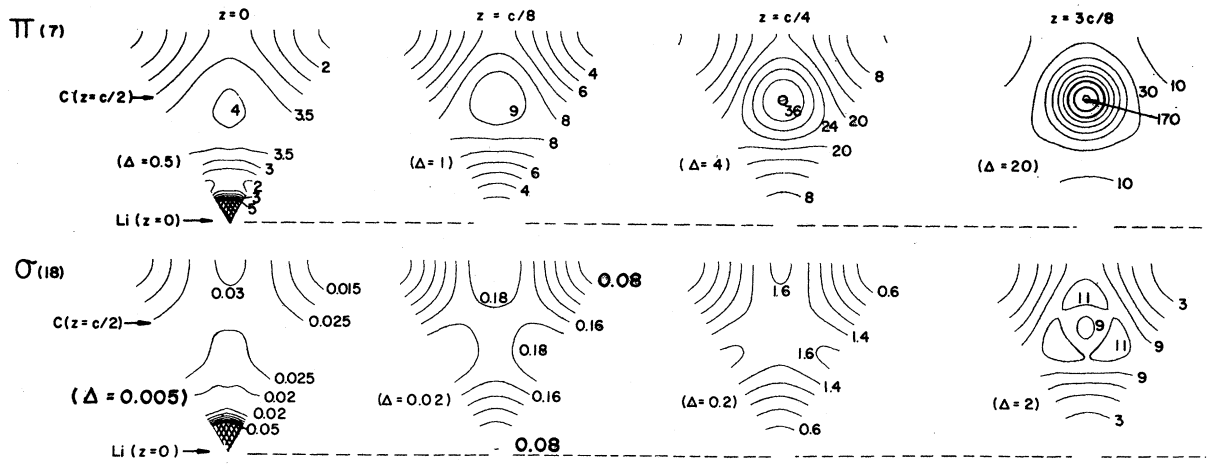

FIG. 5. Contour plots of π and σ partial charge densities in units 10^{-2} e/a.u.^{3} within (smaller) sector indicated in Fig. 1 and in planes as indicated. (Number of electrons per unit cell denoted in parentheses.) Plots for C plane are not included since the π density is essentially 0 and the σ density is essentially equal to total density illustrated in Fig. 2. Contours are equally spaced at intervals Δ.

5 since the π density is essentially zero and the σ density is essentially the same as the total density presented in Fig. 2.

It was suggested in I that the Li 2s state hybridizes with a low-lying bonding C π band to a much larger extent than it does with the Fermi-level C π bands. We are now in a position to visualize this result on the basis of the charge distribution for each type of π band. The types of bands of LiC_6 may be classified by comparison with the π states of benzene.[8] The lowest state of benzene, A, is a bonding state having all π orbitals superposed in phase and it corresponds to the lowest band of LiC_6 which has extrema $\Gamma_2^- - \Delta_1 - A_1^+$. The next-highest states of benzene, E_1 and E_2, are each doubly degenerate. Their wave functions have one and two nodes within the carbon ring and they are termed weakly bonding and weakly antibonding, respectively. These four states correspond to the four Fermi-level bands of LiC_6 which have the extrema $\Gamma_6^+ - \Delta_6 - A_6^-$ and $\Gamma_5^- - \Delta_5 - A_5^+$. In fact, the distinction between E_1-like and E_2-like states in LiC_6 is not precise since a wave function which has one node within a given carbon ring of LiC_6 may have two or more nodes within a neighboring carbon ring. Nevertheless, it is consistent with the available facts to term the lower two Fermi-level bands of LiC_6 "weakly bonding" (E_1) and to term the upper two Fermi-level bands of LiC_6 "weakly antibonding" (E_2). The nodal properties of the three types of occupied π bands of LiC_6 are important for determining the tendency to hybridize with the Li 2s states because they are related to the spatial overlap of the wave functions. Since the Li 2s state is isotropic, it follows that its spatial overlap with the nodeless bonding band of LiC_6 is larger than it is with either the weakly bonding or the weakly antibonding Fermi-level bands. If we can quantify the amount of Li 2s hybridization by the Li contact density we see that the predicted trend is consistent with the calculated results listed in Table I. In particular, of the total contact density of 0.15 e/a.u.^{3}, 53% is contributed by the two electrons in the bonding π band and only 27% by the five electrons in the Fermi-level bands including 6% by the electron in the weakly antibonding π bands. The remaining 20% is contributed by the 18 electrons in σ bands. To investigate possible covalency arising from C π-band–Li 2s hybridization, we consider the partial charge densities of the occupied π bands. In Fig. 6, contour plots for these partial charge densities are given in the small triangular sector denoted in Fig. 1, in the planes

TABLE I. Li contact densities (determined for the crystal potential $Li^+C_6^-$ as described in Sec. II).

Band	Density at Li site
All occupied bands	0.15 (e/a.u.^{3})
Occupied σ bands	0.03
Occupied π bands	0.12
Bonding π band "A"	0.08
Weakly bonding π bands "E_1"	0.03
Weakly antibonding π bands "E_2"	0.01
Unoccupied metal band (if it contained 1 electron)	0.17
Li 2s atom (Ref. 7)	0.21

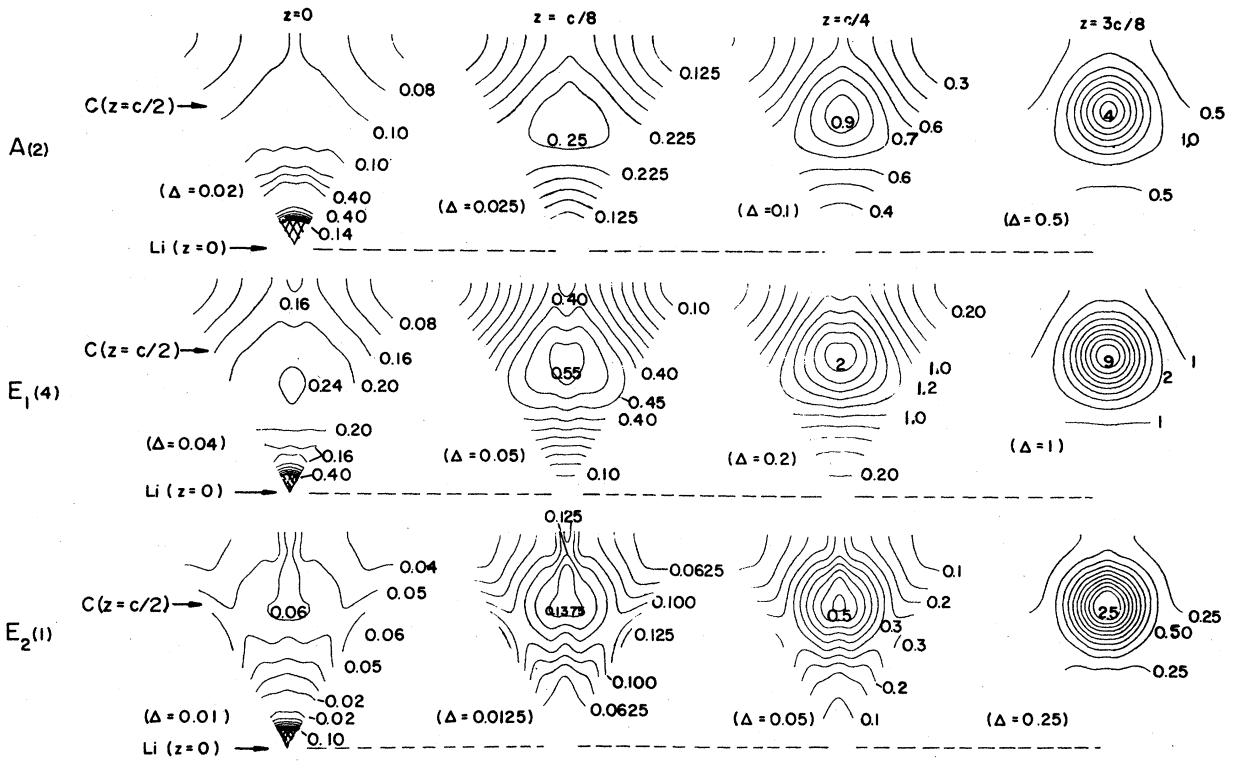

FIG. 6. Contour plots of π-band components of the charge density in units 10^{-2} e/a.u.^{3} within (smaller) sector indicated in Fig. 1 and in planes indicated. Plots for C plane are not included since the density is essentially 0. Components are labeled A, E_1, and E_2 for the bonding, weakly bonding, and weakly antibonding bands, respectively, with the number of electrons per unit cell denoted in parentheses. Contours are equally spaced at intervals Δ.

$z=0$ (Li plane), $\frac{1}{8}c$, $\frac{1}{4}c$ (midplane), and $\frac{3}{8}c$. For each plane the contour values have been chosen to scale with the number of electrons of the three types of bands. In Fig. 6 it is clearly seen that contours for the bonding band A are "attracted" toward the Li site. This is not true for the Fermi-level bands E_1 and E_2, which, as expected, show evidence of nodal contributions along the C-C bonds. The average mean-squared wave function for each of these bands and for the atomic C p_z state are plotted along the C c axis in Fig. 7 (lower panel). The shapes of these curves are very similar and their magnitudes vary according to the bonding and antibonding attributes discussed above.[9] The average mean-squared wave function for the three π bands and for the atomic Li $2s$ state are plotted along the Li c axis in the upper panel of Fig. 7. The π-band wave functions show the characteristic two-peaked structure of a $2s$ density although the magnitude of this feature is reduced by a factor of $\frac{1}{2}$ to $\frac{1}{10}$ from that of atomic Li, all π-band densities passing through zero in the C plane. Of the three π-band densities along the c axis, that of the bonding A band resembles the Li $2s$ density most closely, having peak densities in this direction roughly $\frac{1}{2}$ that of the Li $2s$ density. However, the magnitude of the second peak in the charge density of the A band is reduced by a factor of 4 in a Li plane from its value along the c axis. This highly anisotropic charge distribution associated with the hybridization of the bonding π band of graphite and Li $2s$ states is suggestive of a covalent component to the interlayer bonding.

From the charge-density results, some qualitative comparison with experiment can be made. Experimental results for LiC_6 have been obtained for ^{7}Li NMR spectra[3] and for Raman spectra of phonon modes. Conard and Estrade[3] find the Knight shift for ^{7}Li in LiC_6 to be $\Delta K/K \simeq 0.004\%$, a value which is roughly $\frac{1}{7}$ that of metallic Li.[3] Approximating the Fermi surface average of the Li contact density by the Li contact density due to the average over all states in the two partially filled weakly antibonding E_2 Fermi-level bands listed in Table I, and using the experimental value[10] of the spin susceptibility, we estimate a theoretical value for the Knight shift of LiC_6 to be $\Delta K/K \simeq 0.005\%$, in good agreement with the experimental result.

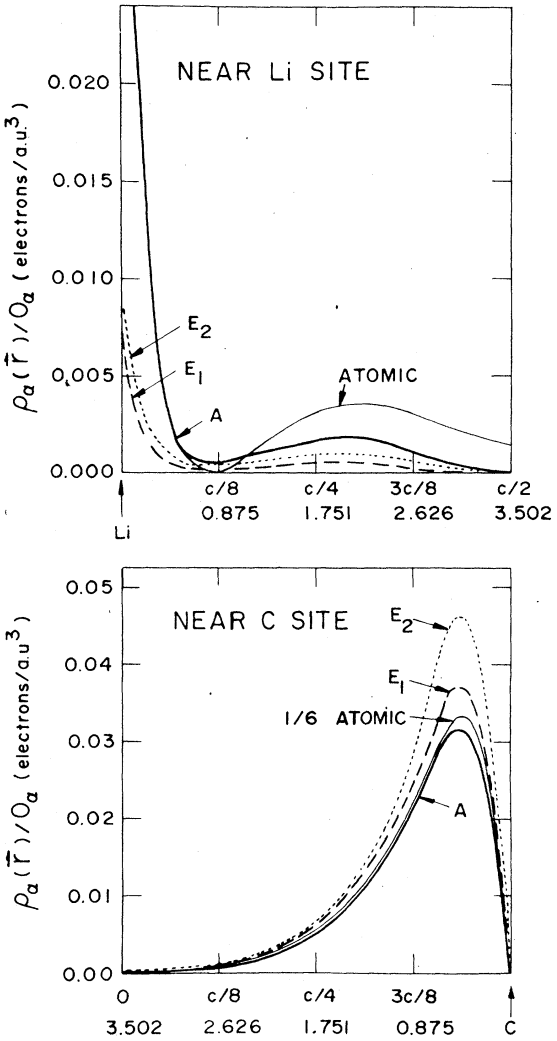

FIG. 7. Average mean-squared wave functions $\rho_\alpha(\vec{r})/O_\alpha$ for bands of LiC_6; bonding band (A, full line), weakly bonding band (E_1, dashed line) and weakly antibonding band (E_2, dotted line); plotted parallel to c axis passing through Li site (upper panel) and through C site (lower panel). Also plotted are the corresponding atomic functions (Ref. 7). In upper panel atomic Li $2s$ squared radial wave function has been multiplied by $(4\pi)^{-1}$. In lower panel atomic C $2p_z$ squared radial wave function has been multiplied by $[\frac{1}{6}\times 3(4\pi)^{-1}]$.

Some qualitative information about differences in C-C cohesive interactions in LiC_6 and graphite is provided by comparison of corresponding lattice constants and of corresponding vibrational frequencies. Guerard and Herold[11] find that the C-C nearest- (intralayer) neighbor distance in LiC_6 is 1% dilated with respect to its value in graphite. Zanini, Ching, and Fischer[4] find that a Raman-active phonon mode involving intralayer C-C stretching, is shifted by 1% to a higher frequency with respect to its value in graphite. Thus, the experimental results for LiC_6 suggest that the intercalation process both lengthens and stiffens the C–C bond. On the basis of the electronic structure of LiC_6, a possible explanation of this effect can be made. If one assumes that the main source of bond alteration in LiC_6 is the additional electron in the weakly antibonding E_2 π bands of graphite, the experimental trend can be understood in terms of the addition of two potential contributions. In the appropriate coordinate system, the effective potential-energy diagram for graphite can be assumed to have a well-defined minimum, while the corresponding potential-energy diagram due to the weakly antibonding bands is undoubtedly repulsive. The repulsive potential-energy contribution is expected not only from the nodal structure of the E_2 states, but also from Coulombic repulsion of the "excess" electron density which is concentrated near each C site. It is easy to imagine that the range of the repulsive potential-energy curve can be such that the sum of the two potential contributions can result in a total effective potential-energy diagram for LiC_6 having a larger C-C equilibrium separation and a more narrow potential well (having greater curvature) than that of graphite. Alternatively, the bond alteration in LiC_6 could be due to the hybridization of the Li and the graphite bands which, as we have seen, mainly affects the bonding A π band of graphite. In this case, one would expect the C-C stretching normal modes to be slightly altered through their coupling with displacements of the Li atoms. Without a detailed study it is difficult to predict on theoretical grounds in which direction such a mechanism would alter bond lengths and vibrational frequencies. However, further experimental studies, such as infrared reflectivity measurements of the C-C stretching modes[12] and neutron-scattering measurements of the interlayer modes,[12] could distinguish between the two possibilities discussed above.

In summary, although the present results have not yet been seriously applied to a study of cohesive properties of LiC_6, they are not in contradiction to the experimental indications available at the present time.

One general question about intercalated graphite compounds is whether or not there is charge transfer between the intercalant and graphitic layers.[2,5] There are structural and thermodynamic data for K, Rb, and Cs donor intercalation compounds[2] which suggest that long-range ionic interactions are important contributions to the binding energy of these compounds.[2] Qualitative features of our results for the valence density

of LiC_6 enable us to address, if not answer this question. For LiC_6, we have firmly established that the electrons associated with the 2s state of atomic Li occupy weakly antibonding π bands of graphite upon intercalation as predicted by a simple rigid-band model. Nevertheless, the physical distribution of charge which is derived from the rigid-band result is not necessarily ionic. As seen in Figs. 4 and 7, the π bands of LiC_6 have peak densities at 0.5 a.u. from each C plane, but have small tails in each Li plane. The magnitude of the density tail of each π band is small, but the total contribution of seven C π electrons for each Li atom has approximately the same order of magnitude as the density which would be contributed by a single atomic Li 2s state. This effect together with the hybrid contribution of the Li 2s state in the A π band indicate that the Li^+ ion is screened in LiC_6 anisotropically but within an average distance smaller than the atomic screening length. This result suggests that long-range Coulomb interactions in LiC_6 are small. In fact, one cannot draw such a conclusion without additional study of the actual binding energy LiC_6. As pointed out by Alonso and Girifalco,[13] the ionic contribution to a binding-energy calculation is not unique, but strongly depends upon the details of the calculation, particularly on one's choice of volumetric partitions. We hope that the present charge-density results will serve to suggest suitable models for future cohesive energy calculations in donor-intercalated graphite compounds.

IV. DISCUSSION

A. Energetic considerations

In Sec. III we demonstrated how the nature of the interaction of the Li and graphite bands could be understood in terms of the forms of the corresponding wave functions. In this section we will consider how the hybridization trends can be also understood in terms of energetic considerations. We can envision two possible ways for the Li 2s band to be formed. One possibility is that the Li 2s band is formed from resonance states that are spatially localized near each Li site. Such a possibility would require a strong local potential near each Li site. In this case, the Li 2s states would form a narrow band energetically located below the maximum energy of the effective one-electron potential of the crystal. A second possibility is that the Li 2s band is formed from highly delocalized states. In this case the local potential near each Li site is not strong enough to cause a 2s resonance; the resulting band would have a metallike width and would be energetically located above all maxima of the effective one-electron potential of the crystal. The results of the band-structure calculation indicate that the second case is operative for LiC_6, suggesting that the potential near a Li site is relatively weak. In contrast, the potential near a C site in LiC_6 is relatively strong. The filled states in the Fermi-level bands are energetically located below the maximum in the crystal potential, and as seen from the charge-density plots presented in Sec. III above, are spatially confined near the C planes. In addition, it is evident that the potential barrier which acts to confine the graphite states near to the C layers is by no means uniform. In particular, in the C-Li direction, the local potential barrier is -1.3 Ry, indicating that a "leakage" of graphite electrons toward the Li site could occur at energies near or above this value. In fact, the low-lying bonding π band of LiC_6 has its minimum at -1.2 Ry; as discussed in Sec. III above, this band has an electron distribution which demonstrates the expected highly directional distortion of graphite charge towards a Li site. The Fermi-level bands of LiC_6 lie at higher-energy eigenvalues than that of the bonding π band, but are even more spatially confined near the C planes as shown in Fig. 7. This trend suggests that the Fermi-level bands are characterized by an increased average kinetic energy component parallel to a C layer, as evidenced by the nodal structures of the charge distributions, with little or no increase in average kinetic-energy component perpendicular to a C layer.

B. Comparison with other donor-intercalation compounds

A point of major interest is whether the electronic properties of LiC_6 are unique or whether similar properties can be expected for MC_8 donor-intercalation compounds, where M=K, Rb, and Cs. As discussed in I, there is both experimental[15–17] and theoretical[18] evidence that MC_8 compounds have some "three-dimensional carriers" in addition to the "two-dimensional carriers" derived from the graphite rigid bands. One of the most direct pieces of evidence for this result, which was used to fix some band-structure parameters in the calculations of Inoshita, Nakao, and Kamimura,[18] is the relatively large ^{133}Cs Knight shift of 0.29% in CsC_8.[15] We note that the relatively large Knight shift for CsC_8 with respect to that of LiC_6 is partly due to the larger atomic number of ^{133}Cs vs ^{7}Li. In fact, the ratio of the Knight shift for CsC_8 to that of Cs metal is only $\frac{1}{5}$, whereas the corresponding ratio for LiC_6 and Li metal is $\frac{1}{7}$. Although the Knight shift depends

upon the spin susceptibility as well as the Fermi contact density, the fact that these ratios are the same order of magnitude would suggest that the metal content of the Fermi-level states for the two materials could be comparable.

The major structural differences between LiC_6 and the MC_8 compounds are due to the increased core size of the heavy alkali metals K, Rb, and Cs with respect to the core size of the Li atom. To zero-order approximation, one would expect the one-electron effective crystal potentials for the MC_8 compounds to be very similar to that of the LiC_6 compound except for the scaling of distances according to the increased metal core sizes. One major difference between the LiC_6 and the MC_8 compounds, however, is due to the fact that the nearest in-plane Li-Li distance in LiC_6 is 30% greater than the nearest Li-Li distance of pure Li metal, whereas the nearest in-plane *M-M* distances of the MC_8 compounds are comparable to the nearest *M-M* distances in the corresponding metals. Therefore, although the distance between nearest-neighbor metal atoms in LiC_6 is smaller than in the MC_8 compounds, the overlap among metal core electrons is less in LiC_6 than in MC_8. Thus, conclusions drawn from the LiC_6 calculation which depend on the small metal core electron overlap may not be valid for the MC_8 compounds. According to the arguments presented above, the smallness of the hybridization between Li and graphite bands is, in fact, partly caused by the smallness of the metal core electron overlap. An increased overlap could increase the hybridization between the metal and the Fermi-level bands by reducing the local potential barriers and generally lowering the potential in each metal plane. The *M* states could then form two-dimensional bands, which for energetic and wave-function overlap reasons could more easily hybridize with the Fermi-level graphite π bands than does the 2*s* state of Li. This trend is seen in the band-structure results for KC_8 of Inoshita, Nakao, and Kamimura,[18] as discussed more fully in I.

C. Self-consistency

By comparing the valence charge density derived from the band-structure calculation with the corresponding density assumed in order to generate the crystal potential, one can get an idea of how the present results differ from self-consistent results. In Fig. 8, the band-structure valence densities (solid lines) which are based on the ionic potential $Li^+C_6^-$, are compared with the corresponding superposed atomic densities for the ionic configuration Li $2s^0$ C $2s^1 2p_{xy}^2 2p_z^{7/6}$ (dashed lines). For contrast, the superposed atomic densities for the neutral configuration Li $2s^1$ C $2s^1 2p_{xy}^2 2p_z^1$ are also included (dotted lines).[5]

The numerically largest difference between the two charge densities occurs near the C site, where the band-structure density is larger than the superposed ionic density. This suggests that a self-consistent potential would screen the C site better than does the $Li^+C_6^-$ potential. Screening of the potential near the C site affects the C σ components of the wave function more than it affects the C π components since the latter are expelled from the immediate vicinity of the C site by the $l=1$ centrifugal potential and also have a node throughout the C plane. On this basis, a self-consistent density would have C components somewhat more extended from the C plane than those of the present results and would have C π components similar to those of the present results. In addition to the discrepancy near the C site, there is a qualitative difference in the shapes of the two densities near the Li site. From Fig. 8 it is apparent that the band-structure density exhibits the cusp and minimum characteristic of the Li 2*s* wave function while the superposed ionic charge density is nearly constant. This difference in shape is due to the fact that the states which compose the band structure density satisfy the Schrödinger equation near the Li site (as well as everywhere else) whereas the states which compose the superposed ionic density do not. On the other hand, the shape of the band-structure density near the Li site is similar to that of the superposed neutral density.

In I, we suggested that the neutral and ionic potential models bracket the relative strength of interactions between the Li and C sites as it would be determined in a self-consistent calculation. If this is correct, we expect the superposed neutral charge density to overestimate the charge near the Li site and the superposed ionic charge density to underestimate the charge near the Li site. The band-structure density should be somewhere between the two model densities. From Fig. 8 it is seen that the expected behavior is exhibited in the immediate vicinity of the Li site (within a sphere of roughly 0.5 a.u.). On this basis, we expect that the self-consistent Li contact density would be smaller than that derived from the present band-structure calculation, in support of the bracketing argument. The comparison of charge densities near a C site is harder to analyze since the differences in the model densities involve the C π states which have nodes near the C site. More generally, a systematic study of the effects of self-consistency should be based

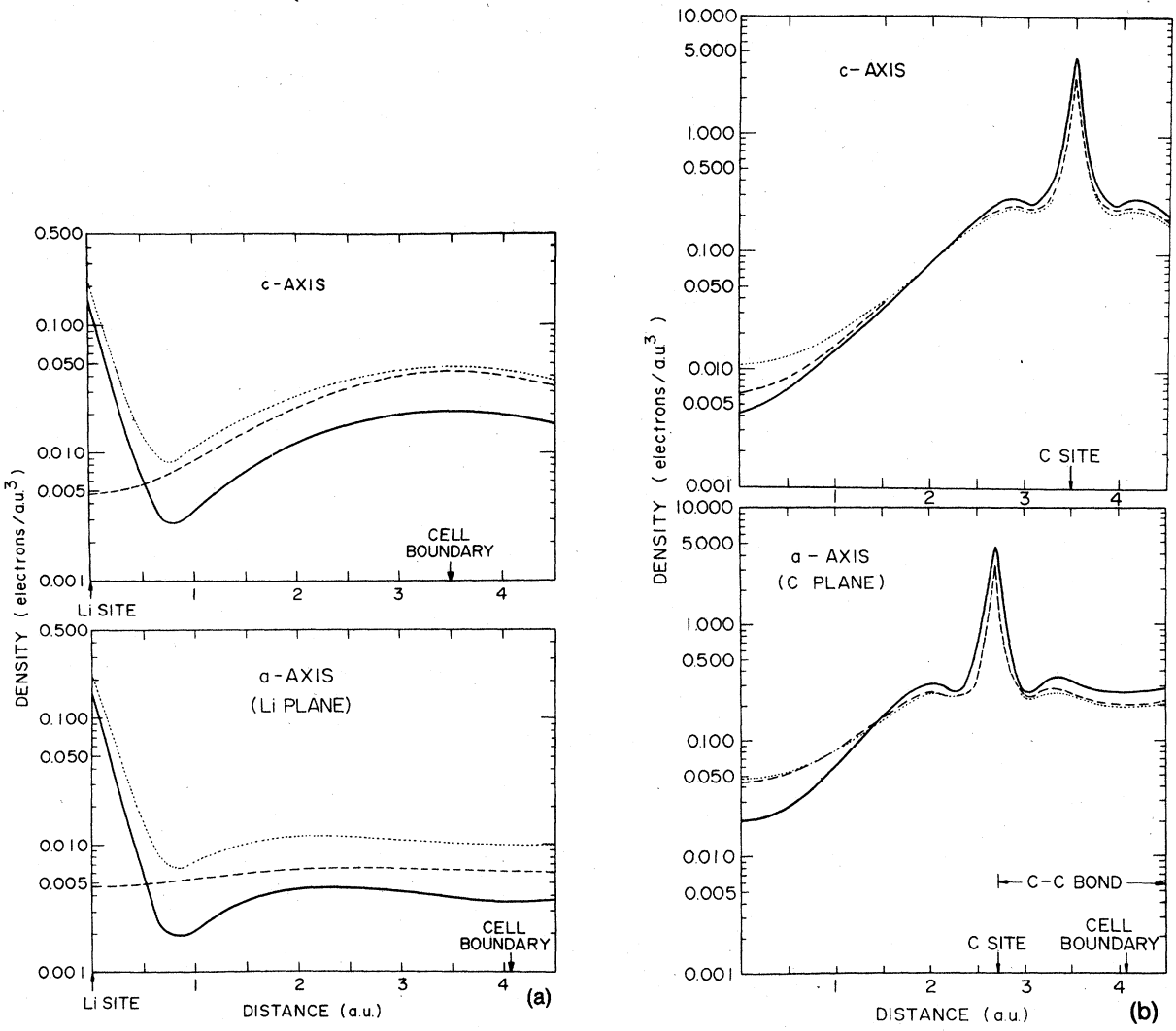

FIG. 8. Total valence charge densities for LiC_6 (full line) compared with corresponding superimposed atomic densities formed from ionic (Li $2s^0$ C $2s\ ^1 2p_{xy}^2 2p_z^{7/6}$ dashed line) and neutral (Li $2s^1$ C $2s^1 2p_{xy}^2 2p_z^1$) (dotted line) configurations. In (a), the c-axis plot starts at a Li atom and passes through the C plane (cell boundary) at the center of a C hexagon while the a-axis Li-plane plot starts at a Li atom and extends along the nearest intralayer Li–Li bond. In (b), the plots are along lines parallel to the (a) plots; the c-axis plot starts at a Li plane below a C atom and passes through a C site, while the a-axis C plane plot starts above a Li site and extends through a C site and then along a C–C bond.

on the comparison of crystal potentials, which is not included in the present work.

D. Summary and conclusions

We have established that the conduction bands of LiC_6 are essentially derived from unoccupied π bands of graphite having peak densities 0.5 a.u. from each C plane and having weakly antibonding character with respect to the C–C bonds. This result is consistent with the experimentally measured Knight shift for ^{7}Li in LiC_6.[3] The conduction properties of such a π band metal are expected to be quite different from those of the more common sp- and d-band metals. In addition to the anisotropy of the Fermi velocities discussed in I, the electron-scattering mechanisms of a π-band metal are expected to be highly anisotropic. Having available the form of the average charge density from the Fermi-level E_2 bands in Figs. 6 and 7 helps us to visualize this effect.

We have also established that the main source of hybridization between graphite and Li states is the low-lying bonding A π band of LiC_6. That the

A band hybridizes to a larger extent than the Fermi-level bands E_1 and E_2, can be understood from the forms of the wave functions, as presented in Figs. 6 and 7, and from energetic considerations discussed in Sec. IV A above. The distortion of charge toward the Li site from the trigonal symmetry about a C c axis suggests that there is some covalent contribution to the binding in LiC_6. Because of their relatively localized spatial extent, the occupied C σ bands are found to be relatively unaffected by intercalation. This is undoubtedly an important factor in determining the stability of a graphite intercalation compound versus that of the corresponding carbide since the C σ bonds are important for maintaining the integrity of the graphite layers.

These qualitative conclusions have been established by means of a detailed band-structure calculation described in Secs. II of Paper I and II of Paper II. While the present results are not self-consistent we have argued in Sec. IV C above that the C π bands and therefore the conclusions discussed above would not be significantly altered if the present results were carried to self-consistency. In addition, we have seen that the present results are consistent with experimental data available at the present time including the specific heat and the optical reflectivity discussed in I and the ^{7}Li Knight shift discussed above. Consequently, we hope that the present results can be used as a basis for constructing models suitable for understanding more complicated physical properties of LiC_6 and related compounds.

ACKNOWLEDGMENTS

We would like to acknowledge stimulating discussions with M. Zanini, J. Alonso, and P. Soven. Our special thanks are also due to the staffs of the David Rittenhouse Laboratory and Moore School computer facilities. This research was supported partially by the National Science Foundation through the University of Pennsylvania Materials Research Laboratory, Grant No. DMR-76-00678, and partially by the Pennsylvania Science and Engineering Foundation, Grant No. PSEF-365.

---

[1]N. A. W. Holzwarth, S. Rabii, and L. A. Girifalco, preceding paper, Phys. Rev. B 18, 5190 (1978). The notation and terminology used in Paper II is the same as that defined in Paper I.

[2]F. J. Salzano and S. Aaronson, J. Chem. Phys. 44, 4320 (1966), and references listed therein.

[3]J. Conard and H. Estrade, Mater. Sci. Eng. 31, 173 (1977).

[4]M. Zanini, L. Y. Ching, and J. E. Fischer, Phys. Rev. B 18, 2020 (1978).

[5]A preliminary report of some of the present results appeared in L. A. Girifalco and N. A. W. Holzwarth, Mater. Sci. Eng. 31, 201 (1977).

[6]D. J. Chadi and M. L. Cohen, Phys. Rev. B 7, 692 (1973); 8, 5747 (1973).

[7]F. Herman and S. Skillman, *Atomic Structure Calculations* (Prentice-Hall, Englewood Cliffs, N.J., 1963). Values quoted for atomic wave functions were obtained from the results of the Herman-Skillman computer program using the α value and atomic configurations used for generating the crystal potential as described in Sec. II of Paper I.

[8]F. A. Cotton, *Chemical Applications of Group Theory* (Interscience, New York, 1963), p. 127ff.

[9]See, for example, C. A. Coulson, *Valence* (Oxford U.P., New York, 1952). Assuming that these bands can be approximately described by a linear combination of atomic orbitals (LCAO), the shape of the feature shown in Fig. 7 is given by the shape of a C $2p_z$ orbital while the magnitude is determined by the inverse of the LCAO normalization constant. Since a bonding state has increased density along a bond, the LCAO normalization constant is larger (and its inverse smaller) than that of an antibonding state. Hence, the feature shown in Fig. 7 should be smallest for the most highly bonding band.

[10]P. Delhaes, J. C. Rouillon, J. P. Manceau, D. Guerard, and A. Herold, J. Phys. (Paris) 37, L-127 (1976).

[11]D. Guerard and A. Herold, Carbon 13, 337 (1975).

[12]M. S. Dresselhaus, G. Dresselhaus, P. C. Eklund, and D. D. L. Chung, Mater. Sci. Eng. 31, 141 (1977).

[13]J. Alonso and L. A. Girifalco (unpublished). See also, R. E. Watson and L. H. Bennett, in *Charge Transfer/Electron Structure of Alloys*, edited by L. H. Bennett and R. H. Willens (Metallurgical Society and American Institute of Mining, New York, 1974), p. 1.

[14]J. C. Slater, *Quantum Theory of Molecules and Solids* (McGraw-Hill, New York, 1965), Vol. 2, p. 309.

[15]G. P. Carver, Phys. Rev. B 2, 2284 (1970).

[16]T. Kondow, U. Mizutani, and T. B. Massalski, Mater. Sci. Eng. 31, 267 (1977).

[17]M. Zanini and J. E. Fischer, Mater. Sci. Eng. 31, 169 (1977).

[18]T. Inoshita, K. Nakao, and H. Kamimura, J. Phys. Soc. Jpn. 43, 1237 (1977).